Top-Down Lipidomic Screens by Multivariate Analysis of High-Resolution Survey Mass Spectra

Dominik Schwudke,[†] J. Thomas Hannich,[†] Vineeth Surendranath,[†] Vinciane Grimard,[†] Thomas Moehring,[‡] Lyle Burton,[§] Teymuras Kurzchalia,[†] and Andrej Shevchenko*,[†]

MPI of Molecular Cell Biology and Genetics, Pfotenhauerstrasse 108, 01307 Dresden, Germany, Thermo Fisher Scientific, 28119 Bremen, Germany, and MDS Sciex, Concord, 71 Four Valley Drive, L4K 4V8 Concord, Canada

Direct profiling of total lipid extracts on a hybrid LTQ Orbitrap mass spectrometer by high-resolution survey spectra clusters species of 11 major lipid classes into 7 groups, which are distinguished by their sum compositions and could be identified by accurately determined masses. Rapid acquisition of survey spectra was employed as a "top-down" screening tool that, together with the computational method of principal component analysis, revealed pronounced perturbations in the abundance of lipid precursors within the entire series of experiments. Altered lipid precursors were subsequently identified either by accurately determined masses or by in-depth MS/MS characterization that was performed on the same instrument. Hence, the sensitivity, throughput and robustness of lipidomics screens were improved without compromising the accuracy and specificity of molecular species identification. The top-down lipidomics strategy lends itself for high-throughput screens complementing ongoing functional genomics efforts.

The full complement of chemically individual lipid species in cells or tissues is termed the lipidome.[1] Lipidomes of eukaryotic cells comprise over a few thousands individual species,[2] which belong to different lipid classes and vary in physicochemical properties, intracellular localization, and abundance. Mass spectrometry plays an important role in the molecular characterization of lipidomes (reviewed in refs 1 and 3−5). Conventionally, molecular species of lipids are identified and quantified via MS/MS experiments, including precursor and neutral loss scans[6−8] or MS^n fragmentation,[9−12] and the determined molecular compositions are compared either directly or using more specific multivariate or cluster analysis.[13]

Fourier transform (FT) mass spectrometers were employed in numerous lipidomics applications.[14−18] High mass resolution, a hallmark of FT analyzers, distinguished *bona fide* lipid peaks from chemical noise and, in some instances, enabled the unequivocal compositional assignment of the resolved isobaric molecular species with no recourse to MS/MS experiments.[19] Despite its recognized potential, the scope of FT MS-driven lipidomics remained rather limited. Sampling of abundant ions of chemical background could exceed the storage capacity of an ion cyclotron resonance (ICR) cell and impair the accuracy of isotopic profiles, thus compromising the species quantification. Inaccurate isolation of precursor ions and poor control over the collision energy hampered the identification or structural validation of matched lipid precursors.[20]

Recently introduced hybrid tandem mass spectrometers combining FT or Orbitrap mass analyzers with a linear ion trap,[21−23] or with a quadrupole,[24] addressed many of the above concerns.[25] Automatic gain control that uses feedback from the ion trap

* Corresponding author: (e-mail) shevchenko@mpi-cbg.de.
[†] MPI of Molecular Cell Biology and Genetics.
[‡] Thermo Fisher Scientific.
[§] MDS Sciex.

(1) Han, X.; Gross, R. W. *Mass Spectrom. Rev.* **2005**, *24*, 367−412.
(2) van Meer, G. *EMBO J.* **2005**, *24*, 3159−3165.
(3) Pulfer, M.; Murphy, R. C. *Mass Spectrom. Rev.* **2003**, *22*, 332−364.
(4) Wenk, M. R. *Nat. Rev. Drug Discovery* **2005**, *4*, 594−610.
(5) Han, X.; Gross, R. W. *J. Lipid Res.* **2003**, *44*, 1071−1079.
(6) Brugger, B.; Erben, G.; Sandhoff, R.; Wieland, F. T.; Lehmann, W. D. *Proc. Natl. Acad. Sci. U.S.A.* **1997**, *94*, 2339−2344.
(7) Ejsing, C. S.; Duchoslav, E.; Sampaio, J.; Simons, K.; Bonner, R.; Thiele, C.; Ekroos, K.; Shevchenko, A. *Anal. Chem.* **2006**, *78*, 6202−6214.
(8) Ekroos, K.; Chernushevich, I. V.; Simons, K.; Shevchenko, A. *Anal. Chem.* **2002**, *74*, 941−949.
(9) McAnoy, A. M.; Wu, C. C.; Murphy, R. C. *J. Am. Soc. Mass Spectrom.* **2005**, *16*, 1498−1509.
(10) Ekroos, K.; Ejsing, C. S.; Bahr, U.; Karas, M.; Simons, K.; Shevchenko, A. *J. Lipid Res.* **2003**, *44*, 2181−2192.
(11) Ejsing, C. S.; Moehring, T.; Bahr, U.; Duchoslav, E.; Karas, M.; Simons, K.; Shevchenko, A. *J. Mass Spectrom.* **2006**, *41*, 372−389.
(12) Larsen, A.; Uran, S.; Jacobsen, P. B.; Skotland, T. *Rapid Commun. Mass Spectrom.* **2001**, *15*, 2393−2398.
(13) Forrester, J. S.; Milne, S. B.; Ivanova, P. T.; Brown, H. A. *Mol. Pharmacol.* **2004**, *65*, 813−821.
(14) Fridriksson, E. K.; Shipkova, P. A.; Sheets, E. D.; Holowka, D.; Baird, B.; McLafferty, F. W. *Biochemistry* **1999**, *38*, 8056−8063.
(15) Ivanova, P. T.; Cerda, B. A.; Horn, D. M.; Cohen, J. S.; McLafferty, F. W.; Brown, H. A. *Proc. Natl. Acad. Sci. U.S.A.* **2001**, *98*, 7152−7157.
(16) O'Connor, P. B.; Mirgorodskaya, E.; Costello, C. E. *J. Am. Soc. Mass Spectrom.* **2002**, *13*, 402−407.
(17) Leavell, M. D.; Leary, J. A. *Anal. Chem.* **2006**, *78*, 5497−5503.
(18) Jones, J. J.; Borgmann, S.; Wilkins, C. L.; O'Brien, R. M. *Anal. Chem.* **2006**, *78*, 3062−3071.
(19) Ishida, M.; Yamazaki, T.; Houjou, T.; Imagawa, M.; Harada, A.; Inoue, K.; Taguchi, R. *Rapid Commun. Mass Spectrom.* **2004**, *18*, 2486−2494.
(20) Jones, J. J.; Batoy, S. M.; Wilkins, C. L. *Comput. Biol. Chem.* **2005**, *29*, 294−302.
(21) Syka, J. E.; Marto, J. A.; Bai, D. L.; Horning, S.; Senko, M. W.; Schwartz, J. C.; Ueberheide, B.; Garcia, B.; Busby, S.; Muratore, T.; Shabanowitz, J.; Hunt, D. F. *J. Proteome Res.* **2004**, *3*, 621−626.
(22) Makarov, A.; Denisov, E.; Kholomeev, A.; Balschun, W.; Lange, O.; Strupat, K.; Horning, S. *Anal. Chem.* **2006**, *78*, 2113−2120.
(23) Hu, Q. Z.; Noll, R. J.; Li, H. Y.; Makarov, A.; Hardman, M.; Cooks, R. G. *J. Mass Spectrom.* **2005**, *40*, 430−443.
(24) O'Connor, P. B.; Pittman, J. L.; Thomson, B. A.; Budnik, B. A.; Cournoyer, J. C.; Jebanathirajah, J.; Lin, C.; Moyer, S.; Zhao, C. *Rapid Commun. Mass Spectrom.* **2006**, *20*, 259−266.

10.1021/ac062455y CCC: $37.00
Published on Web 05/03/2007

analyzer prevents overfilling of the ICR cell or the Orbitrap analyzer and maintains constant peak resolution and better than 2 ppm mass accuracy, irrespective of chemical noise. In MS^n experiments, precursor ions could be accurately isolated by the trap within less than 1.5 Da m/z range and further fragmented either in the same linear trap or in the intermediate C-trap.[26] Better than 100 000 (full width at half-maximum, fwhm) mass resolution of an Orbitrap allows direct identification of fragment ions via their unequivocally determined elemental compositions.[11]

In this study, we demonstrated that direct profiling of total lipid extracts on a LTQ Orbitrap instrument clusters species of 11 major lipid classes into 7 groups, which are distinguished by their sum compositions and could be identified by accurately determined masses. We employed high-resolution survey spectra as a rapid screening tool that, together with the computational method of principal component analysis (PCA), revealed pronounced perturbations in the abundance of lipid precursors. These precursors were subsequently either identified by accurately determined masses or subjected to further MS/MS characterization in the course of the same experiment. Hence, by minimizing the number of required MS/MS spectra, both the sensitivity and throughput were improved without compromising the accuracy and specificity of molecular species identification. The proposed work flow was applied to decipher the global perturbations in eukaryotic lipidomes, induced by free fatty acid feeding and RNAi gene knockdowns.

MATERIALS AND METHODS

Materials and Lipid Standards. Synthetic lipid standards and lipid extracts were purchased from Avanti Polar Lipids, Inc. (Alabaster, AL), Sigma-Aldrich Chemie GmbH (Munich, Germany), and Echelon Research Laboratories, Inc. (Salt Lake City, UT). Water (Lichrosolv grade) was purchased from Merck (Darmstadt, Germany); chloroform, methanol, 2-propanol, and ammonium acetate were of liquid chromatography grade and purchased from Fluka (Buchs SG, Switzerland). Chemical structures and notations of the corresponding lipid classes and species are presented in Supporting Information 3.

Sample Preparation for Mass Spectrometric Analysis. Standards were prepared in the specified concentrations in $CHCl_3$/MeOH/2-propanol 1/2/4 (v/v/v) containing 7.5 mM ammonium acetate. Prior to the analysis, samples were vortexed thoroughly and centrifuged for 5 min at 14 000 rpm on a Minispin centrifuge (Eppendorf, Hamburg, Germany). Samples were loaded onto 96-well plates and sealed with aluminum foil.

Mass Spectrometric Analysis. Analyses were performed on a LTQ Orbitrap hybrid mass spectrometer (Thermo Fisher Scientific, Bremen, Germany) equipped with a robotic nanoflow ion source NanoMate HD (Advion BioSciences Ltd., Ithaca, NJ) with 4.1-μm nozzle diameter chip or, where specified, on a static nano ESI or ESI ion sources (both from Thermo Fischer Scientific). NanoMate HD was controlled by Chipsoft 6.4. software (Advion Biosciences) and operated at the ionization voltage of 1.05 kV and gas pressure 1 psi. When using the nano ESI source, the spraying voltage was adjusted individually within the range of 1.1−1.4 kV. Metal-coated glass needles were from Proxeon Biosystems (Odense M, Denmark) or MasCom Analysengeräte Service GmbH (Bremen, Germany). When using an ESI source, samples were infused at the flow rate of 5 μL/min delivered by a built-in syringe pump and the spraying voltage of 3.8 kV was applied.

MS survey scans were acquired using the Orbitrap analyzer operated under the target mass resolution of 100 000 (fwhm, defined at m/z 400). MS/MS experiments on a LTQ Orbitrap instrument were performed using collision-induced dissociation in the linear ion trap or, where specified, in the intermediate C-trap (termed CID and HCD, respectively) Precursors were selected within the m/z window of 1.5 Da (precursor $m/z \pm 0.75$ Da). Fragment ions were detected by the Orbitrap analyzer operated under the target mass resolution of 30 000 (fwhm, defined at m/z 400). Normalized collision energy was set to 35% for CID and 60% for HCD.

Where specified, MS/MS experiments were performed on a modified QSTAR Pulsar i quadrupole time-of-flight mass spectrometer (MDS Sciex, Concord, Canada) equipped with NanoMate HD ion source. Ionization voltage was set to 0.95 kV, gas pressure to 1.25 psi. Data-dependent acquisition (DDA) experiments were performed as described.[27] The analytical quadrupole Q1 was operated under the unit resolution settings, and fragments were detected in the m/z range of 100−1000 Da. The collision energy offset was 40 eV in all MS/MS experiments.

Data Processing. Using QualBrowser 2.0 software (Thermo Fisher Scientific), each survey spectrum was converted into a peak list, which reported m/z, absolute intensity, relative intensity (normalized to the most abundant peak), and the sum composition for each peak detected with a signal-to-noise ratio above 6 (as determined by QualBrowser). Sum compositions were calculated from the determined precursor masses assuming the following settings: mass tolerance of 4 ppm; even-electron ions; relative double bonds equivalent (RDB) within the range of −1 to 12. Assumed atomic compositions were restricted to the following: nitrogen, 1 to 2 atoms/molecule; oxygen, 2 to 15 atoms; carbon and hydrogen, unrestricted; phosphorus, 0 to 1 atom. Peak lists were saved as comma delimited text (csv) files.

Exported peak lists were further processed by the PECODER (for *pe*ak *co*mbining and *de*isotoping *r*outine) software developed in-house, which is available for download at http://www.scionics.de. PECODER recognized and deisotoped singly charged ions, subtracted background peaks (detected in a separate experiment with the blank sample), and filtered out peaks failing the specified reproducibility criteria. As an output, PECODER produced a table with sum compositions and corresponding intensities detected in all experiments within the series, which was further imported by MarkerView software (MDS Sciex, Concord, Canada) for PCA and *t*-test analysis.

Feeding Fatty Acids to HeLa Cells. Cells were plated on day 1 in a 24-well plate with 1 mL/well of high glucose DMEM supplemented with 10% fetal bovine serum (Invitrogen, Carlsbad, UT). On day 2, wells were spiked with 2 μL of 5 mM solution of different fatty acids in ethanol, such that the final FA concentration was 10 μM. Plates were incubated for 3.5 h at 37 °C at 5% CO_2 (normal growth conditions). The medium was removed and cells

(25) Makarov, A.; Denisov, E.; Lange, O.; Horning, S. *J. Am. Soc. Mass Spectrom.* **2006**, *17*, 977−982.
(26) Olsen, J. V.; de Godoy, L. M.; Li, G.; Macek, B.; Mortensen, P.; Pesch, R.; Makarov, A.; Lange, O.; Horning, S.; Mann, M. *Mol. Cell. Proteomics* **2005**.
(27) Schwudke, D.; Oegema, J.; Burton, L.; Entchev, E.; Hannich, J. T.; Ejsing, C. S.; Kurzchalia, T.; Shevchenko, A. *Anal. Chem.* **2006**, *78*, 585−595.

were rinsed with distilled water. Lipids were extracted using 100 μL of MeOH/$CHCl_3$ 5:1 (v/v) solution and the extract was transferred to a 1.5-mL tube (Eppendorf, Hamburg, Germany). A total of 100 μL of chloroform and 100 μL of water were added, tubes thoroughly vortexed and centrifuged at low speed. The organic phase was transferred into a new 1.5-mL tube and dried down in a vacuum centrifuge.

Preparation of *Caenorhabditis elegans* Lipid Extracts. Wild-type *C. elegans* Bristol N2 worms were grown at 20 °C on NGM (Amp) agar plates for 48 h according to standard procedures.[28] For lipid extraction, ~12 000 worms in M9 buffer[28] (except we replaced 60 mM phosphate buffer with 60 mM ammonium acetate) were disrupted in Mini-Beadbeater-8 with 0.7-mm zirconium beads (Biospec Products, Bartlesville, OK). Lipids were extracted at room temperature essentially as described.[29] Briefly, 1 mL of the lysate was mixed with 3.2 mL of chloroform/methanol 1:2 (v/v). Worm debris was pelleted by low-speed centrifugation on a bench top centrifuge for 15 min at 180*g*. Phase separation was achieved by adding 1 mL of water and 1 mL of chloroform to the cleared supernatant, followed by another 30-min centrifugation at the same speed. The collected organic phase was additionally washed with 2 mL of water. All extraction steps were performed in glassware that was thoroughly washed with water, methanol, and chloroform before use.

RNAi Experiments in *C. elegans*. RNAi for F54D11.1 and ZK622.3 genes was performed in wild-type N2, Bristol strain. F54D11.1 RNAi feeding construct was produced by cloning genomic DNA from 2762 to 3656 bp after the start codon of F54D11.1 with NotI linkers into the NotI site of pPD129.36 (L4440). Subsequently, this construct was used for transforming HT115 *Escherichia coli* used for dsRNA production and feeding.[30] Bacteria for ZK622.3 RNAi were produced using a similar method by MRC GeneService (Cambridge, UK) from the Ahringer dsRNA feeding library.[31] Growing and induction of dsRNA producing bacteria was performed as described[32] with the following modifications: (i) instead of L3-L4 larvae, bleached embryos were subjected to the plates and (ii) isopropyl β-D-1-thiogalactopyranoside was directly mixed with bacteria. Worms fed with bacteria transformed with the empty pPD129.36 (L4440) vector were used as control.

RESULTS

What Lipid Classes Are Distinguishable in High-Resolution Mass Spectra? Let us consider a typical structure of the lipid molecule as a combination of two independent blocks: a lipid-class specific backbone that we further termed as lipid class determinant (LCD) and an aliphatic complement R, comprising methylene (CH_2) and methylidene (CH═CH) groups (Figure 1). Sum compositions of determinants of major lipid classes are presented in Table 1, and corresponding chemical structures are provided in Supporting Information 3.

Mass differences between different LCDs could be balanced by altering the aliphatic complement R. This will produce a series of isobaric lipid species of various classes that, however, differ by their exact masses. For example, the mass difference between the LCDs of PEs and PSs is 43.9898 Da (Figure 1). It can be balanced by changing the aliphatic complement R in two ways, either by adding four CH_2 groups and six double bonds to the structure of PE species or by subtracting three CH_2 groups and adding one double bond to the structure of PS species. The attained exact mass differences equal 0.021 and 0.0726 Da, respectively. We note that, although both options are arithmetically equivalent, they might not occur with the same frequency in endogenous lipids because of natural constraints imposed by lipid biosynthesis pathways. For example, for mammalian isobaric PE and PS species, the latter option is far more common.

In the same way, we computed a matrix of balance masses and corresponding exact mass differences for putative pairs of isobaric species of major lipid classes (Figure 1; Supporting Information 1−3). This matrix allowed us to estimate how the

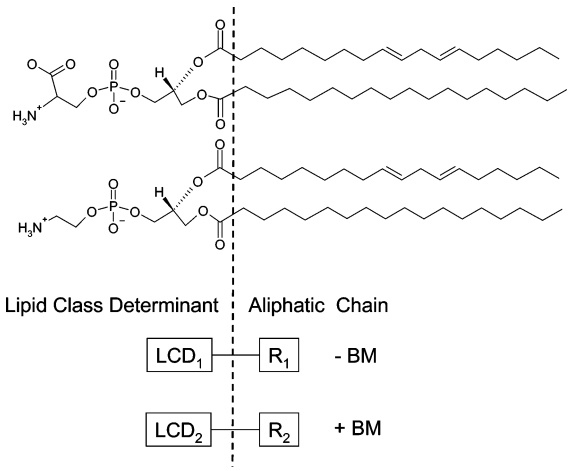

Figure 1. Schematic representation of a typical lipid structure as a combination of LCD and aliphatic complement R. PS 36:2 and PE 36:2 are shown as examples. To compose an isobaric pair of lipids the following conditions are assumed: (i) $(LCD_1 + R_1) - (LCD_2 + R_2 + BM) \rightarrow 0$ and $BM = x_1\,(14.0153) - d_1\,(2.0153)$; or (ii) $(LCD_1 + R_1 - M) - (LCD_2 + R_2) \rightarrow 0$ and $BM = x_2\,(14.0153) + d_2\,(2.0153)$. LCD, lipid class determinant; R, aliphatic chain; BM, balance mass defined by methylene groups and double bonds required to form a pair of isobaric lipid species. x_1, x_2, number of methylene groups, d_1, d_2, number of double bounds added to the BM.

Table 1. Major Lipid Classes Grouped According to Sum Compositions of Their Lipid Class Determinants

lipid group	lipid class[a,b]	C[c]	H	N	O	P
I	PA + NH_4	5	12	1	8	1
	PE + H	7	14	1	8	1
	PC + H	10	20	1	8	1
II	PE-*O* + H	7	16	1	7	1
	PC-*O* + H	10	22	1	7	1
III	PS + H	8	14	1	10	1
	PG + NH_4	8	18	1	10	1
IV	PI + NH_4	11	22	1	13	1
V	SM + H	11	23	2	6	1
VI	TAG + NH_4	6	11	1	6	0
VII	HexCer + H	12	21	1	8	0

[a] Molecular cations commonly detectable in total lipid extracts. [b] Abbreviations and chemical structures are explained in Supporting Information 3. [c] Number of atoms in the backbone.

(28) Brenner, S. *Genetics* **1974**, *77*, 71−94.
(29) Bligh, E. G.; Dyer, W. J. *Can. J. Biochem. Physiol.* **1959**, *37*, 911−917.
(30) Timmons, L.; Fire, A. *Nature* **1998**, *395*, 854.
(31) Kamath, R. S.; Fraser, A. G.; Dong, Y.; Poulin, G.; Durbin, R.; Gotta, M.; Kanapin, A.; Le Bot, N.; Moreno, S.; Sohrmann, M.; Welchman, D. P.; Zipperlen, P.; Ahringer, J. *Nature* **2003**, *421*, 231−237.
(32) Fraser, A. G.; Kamath, R. S.; Zipperlen, P.; Martinez-Campos, M.; Sohrmann, M.; Ahringer, J. *Nature* **2000**, *408*, 325−330.

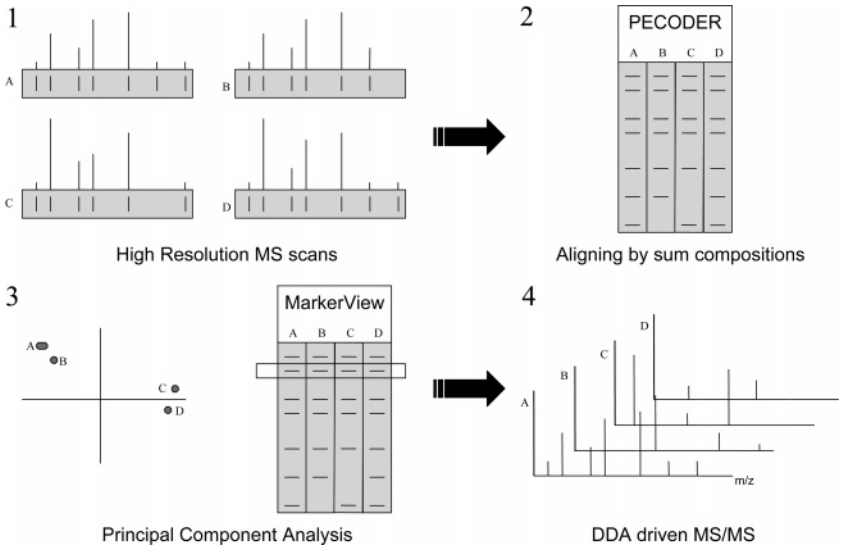

Figure 2. Work flow for high-throughput lipidomics screens. During primary high-throughput screening, high-resolution survey spectra were acquired by direct infusion of total lipid extracts into a LTQ Orbitrap mass spectrometer (panel 1). Spectra acquired from all samples in the series were converted into peak lists and annotated by their calculated sum compositions. PECODER cleaned survey spectra from background, deisotoped peaks, and aligned samples by their sum compositions (panel 2). Subsequent PCA identified the precursors, whose abundances were pronouncedly altered, considering all lipid peak patterns in the entire data set (panel 3). If accurately determined *m/z* did not warrant their unequivocal identification, they were assembled into an inclusion list for the detailed characterization by data-dependent tandem mass spectrometry (panel 4). Importantly, no MS/MS experiments were performed on precursors that either failed the assumed reproducibility criteria, originated from background, or whose abundance changed marginally between analyzed samples and multiple controls.

identification specificity that solely relies on the accurately determined intact lipid masses depends on the actual mass resolution and accuracy. A LTQ Orbitrap mass spectrometer typically delivers the mass resolution of ~100 000 (fwhm) along with better than 3 ppm mass accuracy under the external calibration.[22,33] Assuming that a typical m/z of an "average" lipid is close to 750 Da, in this m/z range the instrument should be able to resolve peaks of the equal abundance spaced by 0.008 Da at 90% height and determine their m/z with an accuracy of 0.002 Da. Hence, it should be possible to distinguish the lipid species whose masses differ by 0.01 Da, depending on the peak abundance ratio and background noise.

We then asked if the resolution of above 100, 000, achievable at high-end FT ICR instruments, would substantially increase the specificity of lipidome profiling. Among 11 major lipid classes, only 2, triacylglycerols (TAGs) and sphingomyelins (SMs) might potentially produce pairs of isobaric species of the smaller mass difference (Supporting Information 2). We note, however, that it is highly unlikely that corresponding endogenous species overlap since the difference of nine methylene groups and five double bonds would be required, implying that at least one of the fatty acid moieties should contain an odd number of carbon atoms. Another close mass difference of 0.009 Da spaces the second isotopic peak of a lipid species and the monoisotopic peak of the species from the same lipid group that lacks one double bond. Computational modeling suggested that, although these peaks were not fully separated under 100 000 resolution, they were still recognized by QualBrowser software and accurate m/z were reported (Supporting Information 4).

With no compositional restrictions applied, 11 common lipid classes could be clustered into 7 sum composition groups that should be unequivocally distinguishable on a LTQ Orbitrap through accurately measured intact masses (Table 1). We reasoned that these measurements might provide sufficiently specific means for taking a fast, yet informative "snapshot" of the lipidome composition, although the exact molecular assignment of certain peaks might remain ambiguous.

To test whether the abundance of peaks detected by Orbitrap survey scans in total lipid extracts warrants the robust quantification, we estimated its dynamic range and detection limit using synthetic lipid standards. To this end, 1,2-di-*O*-phytanyl-*sn*-glycero-3-phosphoethanolamine (PE-*O*-20:0/-*O*-20:0) and D-glucosyl-β1-1′-*N*-dodecanoyl-D-*erythro*-sphingosine (C12 β-D-glucosyl ceramide) were spiked at different concentrations into a bovine heart polar lipid extract, whose concentration remained constant at 0.02 mg/mL. Corresponding calibration curves were linear within the range of 3−2800 nM. The limits of detection calculated at the signal-to-noise ratio of 3 were 4 nM for PE-*O*-20:0/-*O*-20:0 and 7 nM for C12 β-D-glucosyl ceramide (linear fit parameters are presented in Supporting Information 5).

Lipidomic Screens: Work Flow and Proof-of-Concept Experiment. We demonstrated above that direct analysis of total lipid extracts by high mass resolution survey scans reliably distinguished 7 lipid groups corresponding to a total of 11 major lipid classes and that the quantification relying on the intensities of individual peaks was feasible within a wide concentration range. We therefore reasoned that this approach lends itself for rapid, comprehensive and unbiased lipidomics screens (Figure 2).

Typically, peak lists were produced from high-resolution survey spectra that were rapidly acquired from all analyzed samples in the series, including multiple biological and technical replicas and controls. Peak lists were aligned by their m/z, deisotoped, cleaned

(33) Scigelova, M.; Makarov, A. *Proteomics* **2006**, *6*, 16−21.

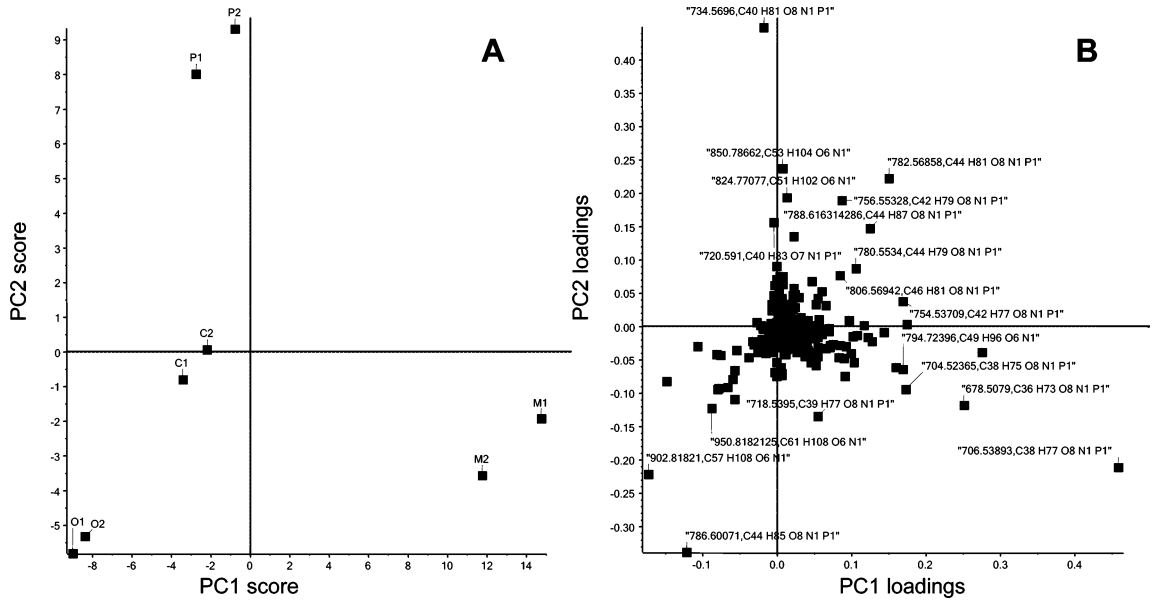

Figure 3. PCA of 262 individual sum compositions detected in HeLa cell feeding experiments. Panel A, PCA plot; panel B, PCA loading plot. M1, M2 stand for two independent experiments with addition of myristic acid; O1, O2, of oleic acid; P1, P2, of palmitic acid; C1, C2, controls, no extra fatty acid added.

from background peaks by the PECODER program, annotated by sum compositions computed from peaks m/z, and submitted to PCA analysis by MarkerView software.

PCA was applied to annotated peak lists produced from all samples in the analyzed series. MarkerView software grouped samples with similar patterns of lipid peaks and also identified pronounced changes between the groups, as judged by their separation in the two-dimensional PCA plot. At the same time, lipid peaks with markedly perturbed intensities were revealed at the loading plot and by their ranking in the principal components, as explained below. Their m/z values were then assembled into an inclusion list for data-dependent tandem mass spectrometric experiments, which subsequently identified and quantified the affected molecular lipid species.

We first applied the approach to decipher the perturbations of the HeLa cells lipidome induced by increased concentrations of palmitic, oleic, or myristic acid in the cell culture media. We anticipated the increased and relatively unbiased incorporation of spiked fatty acids into major cellular lipids[34] and, therefore, reasoned that this could serve as a robust method validation. To this end, we analyzed lipid extracts obtained in eight independent experiments (two for each fatty acid feeding and control) and processed the entire data set as described above.

All four datasets were well separated at the PCA plot (Figure 3A), thus suggesting that the profiled lipidomes were altered substantially and specifically. Sum compositions located off the loading plot center (Figure 3B) had major impact on the variance described by the principal components 1 or 2, according to data points grouping in Figure 3A. Out of, in total, 262 recognized lipid peaks with uniquely assigned sum compositions, using PCA we selected 10 peaks whose relative abundance strongly and specifically increased in different feeding experiments, as compared to the controls (Figure 3B, Table 2).

(34) Kuerschner, L.; Ejsing, C. S.; Ekroos, K.; Shevchenko, A.; Anderson, K. I.; Thiele, C. *Nat. Methods* **2005**, *2*, 39−45.

Candidate lipid precursors revealed by PCA were subjected to MS/MS experiments that determined their molecular composition[27] (Table 2). As anticipated,[34] the abundance of PCs and TAGs comprising the moieties of spiked fatty acids were most enhanced, although the complementary fatty acid moieties varied. We therefore concluded that the proposed screening work flow offers sufficient specificity to identify species, whose abundances altered specifically within the series of experiments. At the same time, clustering of datasets obtained by repetitive analysis, warranted the reproducibility of detected lipid profiles.

Lipidomics Profiling Complements RNAi Screens in *C. elegans*. Although the nematode *C. elegans* is an established model organism in genetics, its potential in lipidomics-driven screens has not yet been explored. RNAi is a powerful reverse-genetics approach used in genome-wide knockdown screens in *C. elegans*. Here we set out to determine if phenotypes produced by RNAi knockdowns can be complemented by in-depth characterization of changes in the worm lipidome. As a pilot proof-of-concept study, we focused on two genes that encoded putative methyltransferases further termed PMT1 (open reading frame (ORF) name ZK622.3) and PMT2 (ORF name F54D11.1), which were both homologous to a family of plant genes implicated in choline biosynthesis.

We characterized lipid profiles in three populations of *C. elegans* worms at the fourth larval stage. In two populations, PMT1 and PMT2 genes were subjected to RNA interference, whereas the third, wild-type population, was used as control. RNAi produced strong visual phenotypes for both gene knockdowns (Figure 4), manifested in decreased body size and uncoordinated movement of affected animals. RNAi of PMT1 and PMT2 genes led to a developmental arrest at the L4/early adult stage and L3 larval stage, respectively.

Total lipid extracts obtained in 18 independent experiments (6 independent repetitions of each RNAi experiment and control) were profiled by high mass resolution survey scans. For each sample, survey spectra were aquired for 2 min within m/z range

Table 2. Relative Intensities of Peaks of Lipid Species Affected by Fatty Acids Feeding, As Revealed by Principal Component Analysis[a]

m/z	sum composition	lipid	M1[b]	M2	O1	O2	P1	P2	C1	C2
706.5389	C38 H77 O8 N1 P1	PC 14:0/16:0	**54.3**[d]	**50.7**	13.7	13.4	14.1	14.1	15.7	16.1
704.5237	C38 H75 O8 N1 P1	PC 14:0/16:1	**7.9**	**7.3**	2.0	2.0	1.7	1.8	2.5	2.6
678.5079	C36 H73 O8 N1 P1	PC 14:0/14:0	**13.3**	**10.8**	0.6	0.5	0.4	0.5	0.7	0.7
794.7240	C49 H96 O6 N1	TAG 14:0/14:0/18:1; TAG 14:0/16:0/16:1[c]	**6.5**	**4.3**	0.2	0.2	0.5	0.3	0.1	0.1
786.6007	C44 H85 O8 N1 P1	PC 18:1/18:1	45.0	44.3	**54.2**	**54.6**	39.5	41.1	45.1	44.7
902.8182	C57 H108 O6 N1	TAG 18:1/18:1/18:1	1.4	1.4	**12.3**	**14.3**	1.9	2.6	2.3	1.9
876.8024	C55 H106 O6 N1	TAG 16:0/18:1/18:1	3.3	3.1	**10.1**	**11.6**	5.6	6.6	3.9	3.2
734.5696	C40 H81 O8 N1 P1	PC 16:0/16:0	34.2	35.8	32.8	31.5	**53.3**	**46.6**	37.4	37.7
824.7708	C51 H102 O6 N1	TAG 16:0/16:0/16:0	1.2	0.9	0.2	0.2	**4.6**	**3.1**	0.4	0.3
850.7866	C53 H104 O6 N1	TAG 16:0/16:0/18:1	3.3	2.8	2.2	2.4	**7.9**	**7.1**	1.6	1.4

[a] Relative intensities are presented in percentage normalized to the most abundant lipid sum composition $C_{42}H_{83}O_8N_1P_1$, subsequently identified as PC 34:1. [b] M1, M2 myristic acid added (FA 14:0); O1, O2 oleic acid added (FA 18:1); P1, P2 palmitic acid added (16:0), C1, C2: controls. [c] Molecular composition of TAGs was determined by MS/MS in positive ion mode; molecular composition of PCs was determined in negative mode as described in ref 27. [d] Abundances of species specifically enhanced by fatty acid feeding are in bold.

of 500−1000 Da. A total of 112 sum compositions (excluding TAGs) were submitted to PCA (Supporting Information 6). Although TAG accumulation was also deficient, it was considered as a secondary phenotype induced by in-depth perturbation of the membrane lipidome. All three populations were clearly separated at the PCA plot (Figure 4A), while the loading plot (Figure 4B) revealed that the lipidomes of control worms and of both RNAi populations underwent a complex change in relative abundances of several sum compositions.

Sum compositions having a major effect on the separation of populations are highlighted at the loading plot (Figure 4B) and presented in the candidate list (Table 3). As a representative example of each population, the abundance of peaks corresponding to three sum compositions, $C_{45}H_{79}O_8N_1P_1$ for area I, $C_{44}H_{85}O_8N_1P_1$ for area II, and $C_{43}H_{81}O_7N_1P_1$ for area III, are presented in Figure 4. These candidate sum compositions belonged to groups I and II (Table 3) and could be assigned to several lipid classes that are indistinguishable by accurate mass measurements, and therefore, correspondent precursors were subsequently characterized by MS/MS.

In L4x samples (wild type), sum compositions that belonged to $C_xH_yN_1O_8P_1$ group found in area II (green) were identified by MS/MS as phosphatidylcholines (Table 3). For example, the precursor *m/z* 806.5696 with the sum composition $C_{46}H_{81}N_1O_8P_1$ was identified as PC 38:6 and its abundance was decreased in both RNAi knockdown populations.

The abundance of precursors with *m/z* 792.5542 (Figure 4, panel I and Table 3, first row) and 756.5542 (Table 3, seventh row) was substantially increased in the PMT2x knockdown population. MS/MS experiments were performed on the same precursors detected in total extracts of the wild-type and PMT2x knockdown worms (Figure 5A,B). While the precusor *m/z* 792.5542 comprised only PC 37:6 in the control (Figure 5A), two new abundant peaks with *m/z* 170.0507 and 623.5035 (designated with arrows) were observed in the corresponding MS/MS spectrum in PMT2x knockdown sample, which were assigned as specific fragments of the dimethylphosphatidylethanolamine (DMPE) headgroup (Figure 5B). Similarly, precursor *m/z* 756.5542 comprised both PC 34:3 and PE 37:3 in the control sample (Figure 5C). However, additional fragments with *m/z* 601.5205 and 587.5045 that corresponded to neutral loss of monomethylphosphatidylethanolamine (MMPE) and DMPE head groups, respectively (designated with arrows in Figure 5D) were also detected. DMPE or MMPE species were detected in all candidates precursors from area I (Figure 4). We therefore reasoned that the increased abundance of peaks in area I in the PMT2x knockdown series could be explained by the accumulation of MMPE and DMPE species.

To validate these findings, we performed an independent DDA-driven experiment[27] on a QSTAR Pulsar *i* mass spectrometer (Figure 6) and also analyzed extracts by TLC (Supporting Information 7). In full concordance with the outcome of the high mass accuracy screen, both methods confirmed the accumulation of MMPE and DMPE species. The plot of relative abundances of lipid species identified by the DDA-driven experiment is presented in Figure 6, in which precursors also recognized by the high mass accuracy (HMA)-driven screen are designated with arrows. In total, 72 MMPE and DMPE species were detected by DDA-driven profiling in the lipid extract of the RNAi knockdown worms, while they were absent in the wild type. Thirteen lipid species were directly recognized by survey scan screens, despite many of them overlapping with peaks of PC and PE species having the same exact masses. Figure 6 indicates that survey scan screens might be biased towards discovering intense peaks that, preferably, do not overlap with abundant species from other nonaffected lipid classes. This, however, could be compensated at the stage of the secondary DDA-driven MS/MS screening by expanding the inclusion list beyond *m/z* of top candidates suggested by PCA (Figure 6).

Within the PMT1x population of worms, the realtive abundance of species that belong to lipid group II (sum compositions $C_xH_yN_1O_7P_1$) increased, while, similar to PMT2x knockdowns, the relative abundance of PC species decreased. MS/MS experiments, performed as described above, also suggested the increase in the relative abundance of species $C_xH_yN_1O_7P_1$ group in area III (Figure 5), which, in this case, consisted mainly of PE-ethers (data not shown). We, therefore, concluded that phosphoethanolamine methylation pathway(s) was (were) perturbed in PMT1 RNAi treated worms and that this gene product might also function as a methyltransferase. However, since intermediate products (MMPE

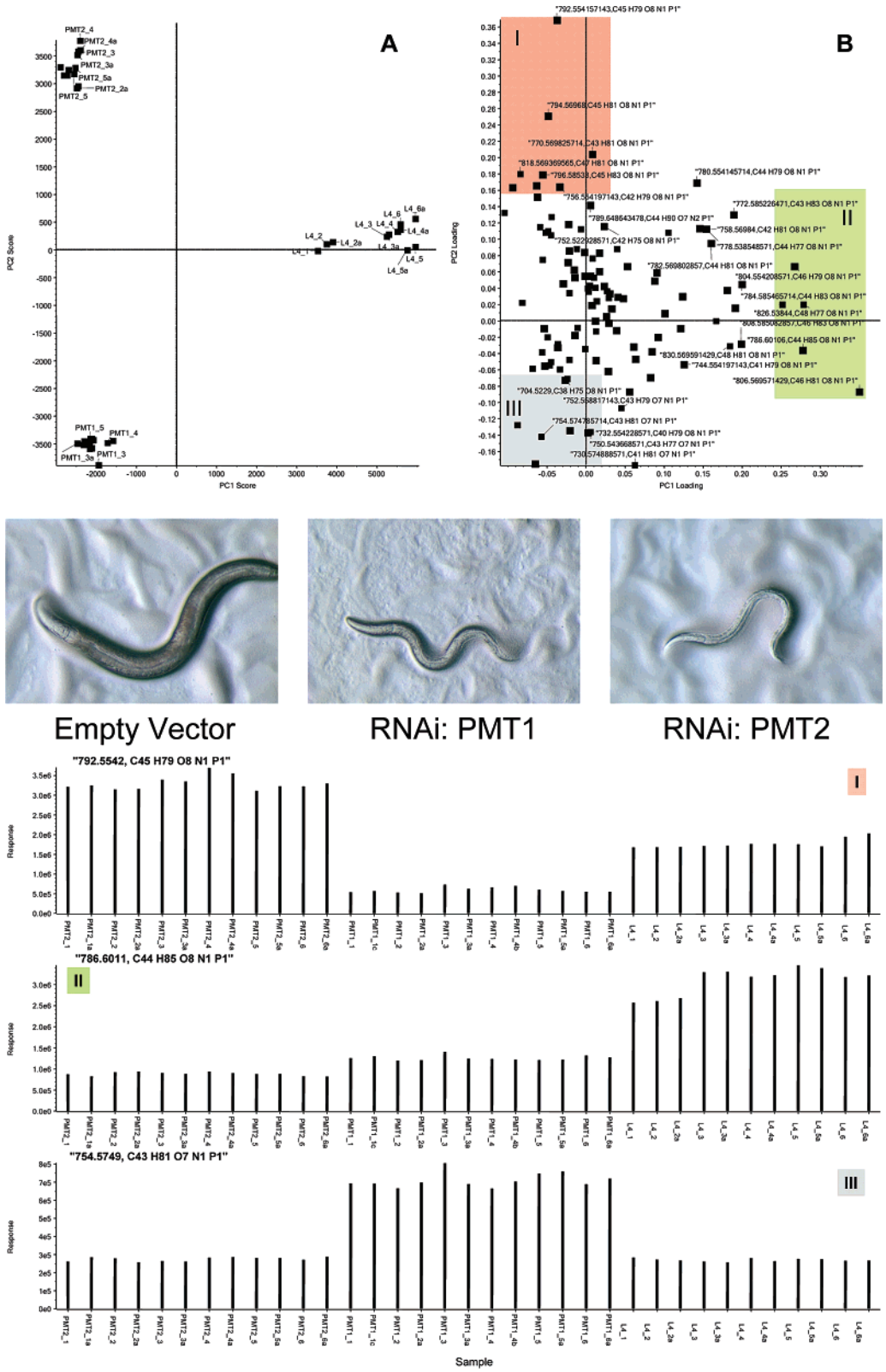

Figure 4. PCA of 3 populations of *C. elegans*: L4x, control, lipid extract from wild-type worms in fourth larval stage; PMT2x-RNAi of gene F54D11.1; and PMT1x-RNAi of gene ZK622.3. The symbol x indicates the number of the replicate spectrum repetitively acquired from the same extract. Data were acquired from 18 lipid extracts (6 for each population). All samples were measured twice except L41. Intensity threshold for signal-to-noise ratio was set to 6, and only sum compositions that were detected in, at least, 50% of all analyzed samples were considered. Analysis was consecutively performed on 112 unique sum compositions (excluding TAGs). Intensities were normalized to the combined intensities of all peaks attributed to lipid group I ($C_xH_yN_1O_8P_1$). PCA analysis was performed with MarkerView software by using Pareto scaling method and PCA weighting was set to None. (A) PCA plot; (B) loading plot with the representative pictures of RNAi treated animals showing strong phenotypic changes. Areas I (red), II (green), and III (gray) highlight groups of sum compositions with increasesed relative abundance specific for one population I, PMT2_x; II, L4_x; and III, PMT_1x. I: relative abundance of the peak with *m*/*z* 792.5542 ($C_{45}H_{79}O_8N_1P_1$), representative for red shaded region. II: relative abundance of *m*/*z* 786.6011 ($C_{44}H_{85}O_8N_1P_1$), representative for green shaded region. III**:** relative abundance of *m*/*z* 754.5749 ($C_{43}H_{81}O_7N_1P_1$), representative for gray-shaded region.

Table 3. Sum Compositions Responsible for Separation of Lipid Profiles in *C. elegans* Knockdown Populations and Control[a]

			L4		PMT1		PMT2	
m/z	sum composition	lipid group	abundance × 10^4	rel Stdev (%)	abundance × 10^4	rel Stdev (%)	abundance × 10^4	rel Stdev (%)
			Area I					
792.5542	C45 H79 O8 N1 P1	I	176.4	6.5	59.3	11.8	330.2	5.3
794.5697	C45 H81 O8 N1 P1	I	128.7	3.5	85.8	8.0	215.7	6.7
770.5698	C43 H81 O8 N1 P1	I	108.3	7.4	59.7	7.8	142.1	4.0
818.5694	C47 H81 O8 N1 P1	I	3.3	11.5	nd	-	76.2	5.8
796.5854	C45 H83 O8 N1 P1	I	53.1	4.6	38.9	7.5	108.1	7.7
814.5374	C47 H77 O8 N1 P1	I	8.6	19.5	nd	-	61.1	6.0
756.5542	C42 H79 O8 N1 P1	I	60.3	9.9	42.9	11.2	99.1	3.9
790.5380	C45 H77 O8 N1 P1	I	6.8	8.2	11.2	21.1	78.3	4.8
			Area II					
806.5696	C46 H81 O8 N1 P1	I	722.1	8.9	447.3	7.4	350.2	3.1
826.5384	C48 H77 O8 N1 P1	I	366.7	8.7	156.4	33.4	157.1	3.6
786.6011	C44 H85 O8 N1 P1	I	309.9	10.4	125.6	4.8	88.0	4.7
804.5542	C46 H79 O8 N1 P1	I	264.5	8.5	50.8	36.4	82.3	6.7
828.5538	C48 H79 O8 N1 P1	I	290.8	6.7	121.2	17.5	123.0	4.7
784.5855	C44 H83 O8 N1 P1	I	206.0	8.3	89.9	7.2	104.9	2.7
808.5851	C46 H83 O8 N1 P1	I	276.0	7.7	182.3	7.3	161.1	6.0
			Area III					
812.6556	C47 H91 O7 N1 P1	II	22.5	17.6	94.2	20.4	43.7	5.9
754.5748	C43 H81 O7 N1 P1	II	26.9	3.1	71.0	5.8	27.4	4.1
732.5542	C40 H79 O8 N1 P1	I	68.2	4.8	88.9	8.0	50.7	2.6
750.5437	C43 H77 O7 N1 P1	II	48.5	7.0	67.8	6.7	30.5	4.0
742.5386	C41 H77 O8 N1 P1	I	56.7	6.2	85.9	17.8	45.9	1.3
728.5593	C41 H79 O7 N1 P1	II	37.0	7.2	92.4	6.6	51.7	4.6
704.5229	C38 H75 O8 N1 P1	I	19.5	6.8	32.1	6.8	19.1	31.7
726.5438	C41 H77 O7 N1 P1	II	3.9	9.7	13.9	10.7	3.2	9.4

[a] I, II, and III are the areas in loading plot Figure 6B. Lipid group assignment is based on sum compositions according to Table 1.

and DMPE) were not detected, we reasoned that PMT1 protein might be involved in the first methylation step.

Since in both RNAi knockdown experiments relative abundance of PC species was decreased, compared to the control, this supported a notion that PMT1 (ZK622.3) and PMT2 (F54D11.1) are, indeed, methyltransferases and are presumably involved in the biosynthesis of phosphatidylcholine. PMT1 gene, whose knockdown did not result in the accumulation of methylation intermediates, is most likely responsible for the first methylation step. At the same time, PMT2 gene, whose knockdown triggered the accumulation of both MMPE and DMPE, is likely responsible for the second and third methylation steps. This was independently confirmed by the transformation of the corresponding *C. elegans* genes into yeast strains and complementation of phosphatidylcholine biosynthesis mutant phenotypes (data not shown). In addition, the phenotypes in RNAi knockdown animals were rescued by adding choline for PMT1 and PMT2 and monomethylethanolamine or dimethylethanolamine for PMT1 (data not shown). In the course of our investigation, another group has independently identified PMT2 as a phosphomethylethanolamine methyltransferase, which produces phosphocholine.[35] Phosphocholine can be directly used in the Kennedy pathway to produce phosphatidylcholines.

(35) Palavalli, L. H.; Brendza, K. M.; Haakenson, W.; Cahoon, R. E.; McLaird, M.; Hicks, L. M.; McCarter, J. P.; Williams, D. J.; Hresko, M. C.; Jez, J. M. *Biochemistry* **2006**, *45*, 6056−6065.

Taken together, our results demonstrated that high mass resolution survey scans could be applied for unbiased, rapid, and accurate characterization of perturbations in complex eukaryotic lipidomes. Importantly, the method solely relies on the identification of changes in abundances of detectable lipid peaks and does not require any preliminary hypothesis on which lipid classes could be affected.

DISCUSSION

Conventional mass spectrometry-driven lipidomics screening typically follows a classic "bottom-up" analytical strategy. It starts with the identification and quantification of individual molecular species (such as PC 18:0 /16:1) or, more frequently, lipids of the same class and sum composition (like PC 34:1, without specifying the fatty acid moieties) and summing up their contents to reveal global changes within the whole lipidome. These differences are rarely global, but are frequently confined within a class or a few lipid classes, whereas deviations in the abundance of other lipid species are marginal. Often, lipidomics screens reveal no specific changes for purely technical reasons, such as insufficient amounts of recovered lipids, unstable analysis conditions, or heavy contamination of analyzed samples. This, however, only becomes clear at the final stage of data interpretation, and in any case, and therefore it is required that spectra acquisition and processing are performed with utmost care, which is always labor intense and not always practical.

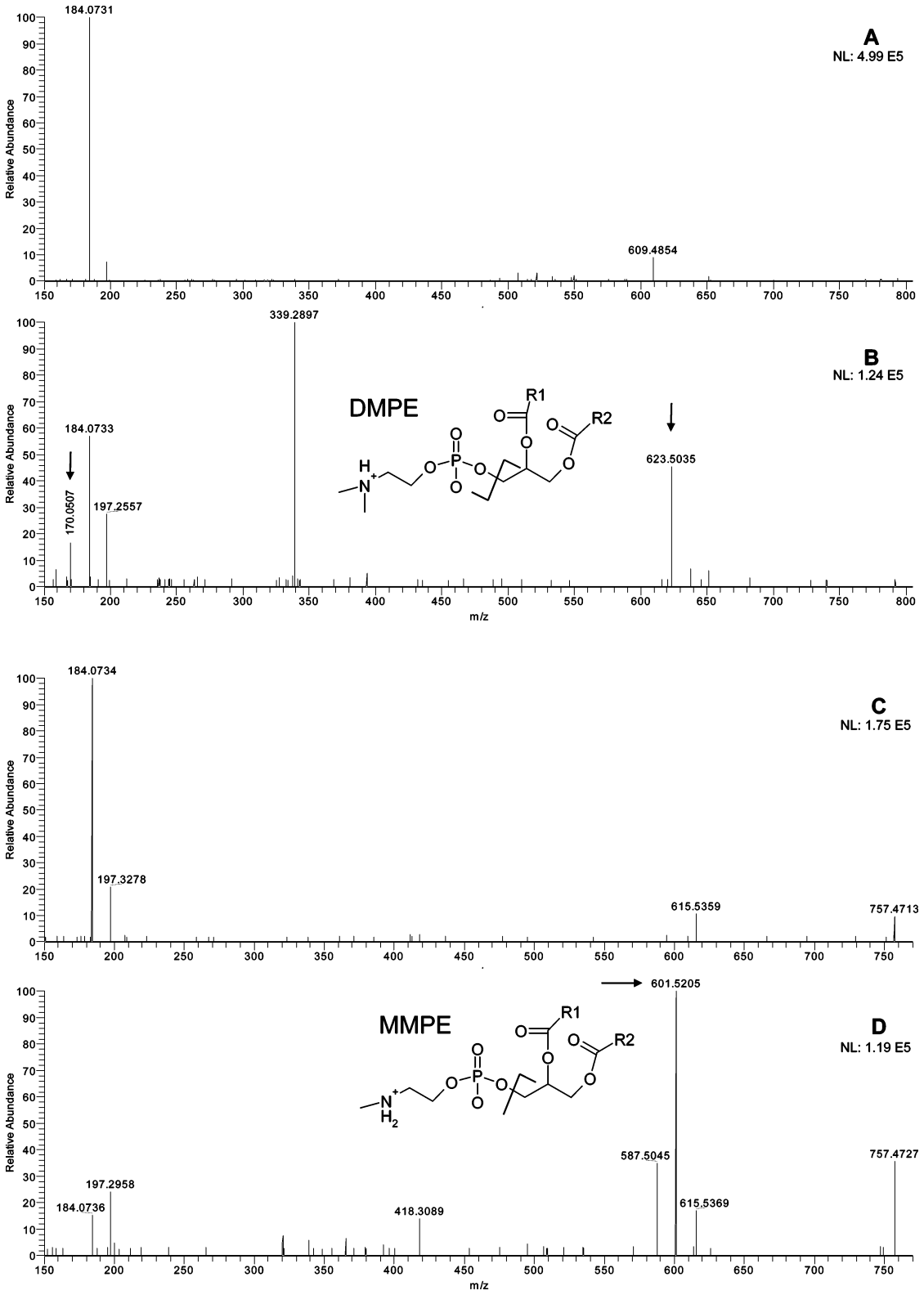

Figure 5. MS/MS analysis performed in HCD mode on a LTQ Orbitrap instrument on precursors from the area I (Table 3). Panels A and B: spectra acquired from *m*/*z* 792.5542 (sum composition $C_{45}H_{79}O_8N_1P_1$) in L4x and PMT2x series, respectively. Panels C and D: spectra acquired from *m*/*z* 756.5542 (sum composition $C_{42}H_{79}O_8N_1P_1$) in L4x and PMT2x series, respectively.

Here we proposed an alternative top-down lipidomics screening strategy, which contrasts the conventional approaches in several ways. First, we always acquire a complete data set of survey spectra from all samples within the series of experiments. Therefore, subsequent PCA is far more specific than any pairwise comparison between analyzed samples and control(s). Second, we do not employ MS/MS experiments as a primary high-throughput screen and, hence, benefit from the improved sensitivity, throughput, and also robustness of the analysis because it is not any longer required to maintain perfect spraying stability over

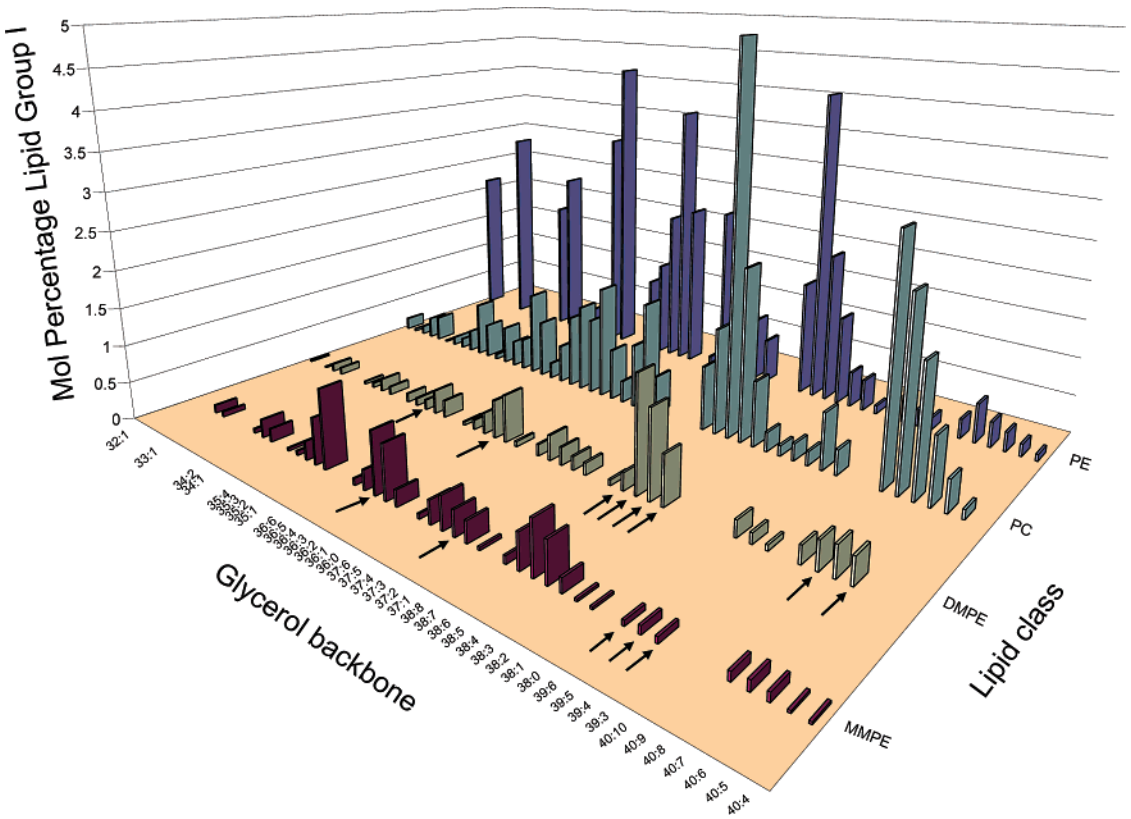

Figure 6. Lipid profiles of PMT2x RNAi knockdown worms. Phoshatidylethanolamine (PE), MMPE, DMPE, and phoshatidylcholine (PC) profiles were determined by DDA-driven profiling. Lipids that were identified by the HMA screen are designated by arrows.

a long period of the acquisition time. A single high-resolution survey spectrum with good ion statistics could be acquired within a minute, whereas complete analysis by multiple precursor ion scans[7,10] or DDA[27] typically requires more than 30 min under perfectly stable spraying. We also note that both MS/MS-driven methods would miss even abundant precursors from lipid classes, which were unexpected in the analyzed mixture, and therefore, m/z of corresponding characteristic fragments, neutral losses, or both had not been preselected in the acquisition or interpretation software. High specificity of survey scan screening was achieved by a high mass resolution Orbitrap analyzer (>100 000 fwhm), which divided the entire pool of major lipids into seven groups. The identity of affected molecular lipid species was then established by targeted MS/MS analysis that only encompassed a small number of selected precursors and could be cross-checked for the presence of unanticipated fragment ions rendered from yet unrecognized molecular species. We also note that, for several lipid classes, lipid species could be identified solely by their intact masses hence requiring no further MS/MS. Robotic nanoflow sample infusion systems, together with the high instrument sensitivity, enabled performing both MS and targeted MS/MS analysis on the same LTQ Orbitrap instrument using the same samples placed into a 96-well plate.

However, one should also consider that high throughput and ease of use of top-down screens comes at the price of, by definition, incomplete detection of all relevant species. Despite highly accurate informatics procedures, the primary screen is intrinsically biased towards reporting intense, strongly affected peaks since these would be expected to mostly contribute to the differences in acquired signal patterns. Highly specific changes in minor peaks that happened to overlap with intense peaks of isomeric compounds might not be revealed by PCA at all. It is therefore advisable to expand the inclusion lists for DDA-driven MS/MS by considering m/z of other members of the affected lipid class(es) during the in-depth secondary screen. In practice, this constitutes less of a problem since the major goal of primary screens is rapid selection of samples with interesting changes in their lipidome, rather than precise and comprehensive identification of all affected molecules.

Being rapid and sufficiently specific, the approach, nonetheless, required high-quality sample preparation. For example, varying intensity of sodium (in positive ion mode) or chloride (in negative ion mode) adducts affected the PCA specificity. This, however, was addressed by a carefully executed lipid extraction, including additional washing steps to decrease salt-related background. First, we washed cell pellets prior to lipid extraction to remove buffer components (often used in the 100 mM concentration range) with 150 mM ammonia acetate and, hence, decreased the overall salt content in the extracted media. Second, when following classic Bligh and Dyer extraction procedure,[29] we additionally washed with water the collected organic phase containing recovered lipids. Third, we performed all extraction steps in glassware, which were thoroughly washed, successively, with water, methanol, and chloroform, but not with detergents. While preparing samples for direct infusion nanoflow analysis, it is important to operate with appropriately diluted analytes. In our experience, the total lipid concentration should not exceed (very approximately) 50 μM, while the concentration of major lipid species should be maintained below 1 μM.

We applied top-down screening to elucidate the function of two genes in *C. elegans* having plausible methyltransferase activity. We note that the composition of the glycerophospholipidome in worms is quite unusual since the species often comprise polyunsaturated fatty acids and fatty acids with odd numbers of carbon atoms.[36] Nonetheless, the high mass resolution screening allowed us to confine the lipidome perturbations to a single sum composition group. Secondary screen by DDA-driven MS/MS and automated interpretation of tandem mass spectra acquired from the perspective precursors identified the accumulated lipid intermediates and helped to elucidate the function of both genes within phosphatidylcholines synthesis pathways.

Taken together, top-down mass spectrometric screening proved to be a powerful tool that is capable of complementing genetic screens by rapid and direct profiling of cellular lipidomes.

CONCLUSIONS AND PERSPECTIVES

Despite the recent progress in bioinformatics, functional genomics, and proteomics, functional annotation of ORFs uncovered by genomic sequencing in many popular model organisms remains a challenging problem. Gene manipulation technologies like RNAi[30] can produce functional gene knockdowns at the genome-wide scale at a very high speed. However, the characterization of the molecular background of observed phenotypes remains a significant bottleneck.[31] Because of the complexity of cellular lipidomes and high redundancy of lipid biosynthesis pathways, this is particularly important in the functional characterization of lipid metabolism genes.[37,38] Therefore, lipidomics technologies that, by their scalability, sensitivity, and scope, match the performance of genome-wide genetic screens could play a big role in uncovering the molecular mechanisms of numerous metabolism-related disorders.

To achieve the desired genome-scale throughout, several further developments in the proposed top-down screening methodology are required. First, PCA should be back-integrated to raw mass spectrometric data such that it should become possible to control DDA-driven mass spectrometric experiments in real time. In addition, better understanding of the compositional divergence of lipidomes in various biological contexts would help to fine-tune the statistical methods towards accurate description of complex metabolomics and lipidomics datasets. Along the same lines, a generic software should be developed for interpreting MS/MS lipidomics data, which would utilize user-defined algorithms for the identification and quantification of molecular lipid species. When combined with a new generation of high mass resolution instruments, the technology should provide a much-sought bridge between genomics, lipidomics, and cell biology.

(36) Tanaka, T.; Izuwa, S.; Tanaka, K.; Yamamoto, D.; Takimoto, T.; Matsuura, F.; Satouchi, K. *Eur. J. Biochem.* **1999**, *263*, 189−195.
(37) Watts, J. L.; Browse, J. *Proc. Natl. Acad. Sci. U.S.A.* **2002**, *99*, 5854−5859.
(38) Brock, T. J.; Browse, J.; Watts, J. L. *PLoS Genet.* **2006**, *2*, e108.

ACKNOWLEDGMENT

We are grateful to Prof. Kai Simons (MPI CBG) and Dr. Michaela Scigelova (Thermo Fisher Scientific, San Jose, CA) for useful discussions on lipidomic strategies; to members of Shevchenko laboratory their expert support; Dr. Eugeni Entchev for expert support in RNAi experiments; and Ms. Judith Nicholls (MPI CBG) for critical reading of the manuscript. This project was supported by SFB/TR 13 grant from Deutsche Forschungsgemeinschaft to A.S. (project D1) and T.K. (project B2).

SUPPORTING INFORMATION AVAILABLE

Additional information as noted in text. This material is available free of charge via the Internet at http://pubs.acs.org.

Received for review December 29, 2006. Accepted March 27, 2007.

AC062455Y